

A Monte Carlo study of the dependence of early frame sampling on uncertainty and bias in pharmacokinetic parameters from dynamic PET

Ida Häggström¹, Jan Axelsson¹, C Ross Schmidtlein², Mikael Karlsson¹, Anders Garpebring¹, Lennart Johansson¹, Jens Sörensen³ and Anne Larsson¹

¹Department of radiation sciences, Umeå University, Umeå, Sweden
SE-901 87 Umeå, Sweden

²Department of medical physics, Memorial Sloan-Kettering Cancer Center, New York, USA
New York, NY 10065, USA

³Nuclear medicine and PET, Dept. of radiology, Oncology and radiation sciences, Uppsala University, Uppsala, Sweden
SE-751 85 Uppsala, Sweden

Corresponding, first author:

MSc. Ida Häggström
Department of radiation sciences, radiation physics
Umeå University
SE-901 87 Umeå
Sweden

Email: ida.haggstrom@radfys.umu.se

Telephone: +46(0)90-7852784

Abstract word count: 292

Text word count: 5976

Short title: Effect of frame sampling on PET kinetics

ABSTRACT

Compartmental modeling of dynamic PET data enables quantification of tracer kinetics *in vivo*, through the calculated model parameters. In this study the aim was to investigate the effect of early frame sampling and reconstruction method on pharmacokinetic parameters obtained from a 2-tissue model, in terms of bias and uncertainty (standard deviation, SD).

Methods: The GATE Monte Carlo software was used to simulate 2×15 dynamic ^{18}F -FLT brain PET studies, typical in terms of noise level and kinetic parameters. The data was reconstructed by both three-dimensional (3D) filtered back-projection with reprojection (3DRP) and 3D ordered subset expectation maximization (OSEM) into six dynamic image sets with different early frame durations of 1, 2, 4, 6, 10 and 15 s. Bias and SD were evaluated for fitted parameter estimates, calculated from region-of-interests.

Results: The 2-tissue model parameter estimates K_1 , k_2 , and V_a depended on early frame sampling, and a sampling of 6-15 s generally minimized bias and SD. The shortest sampling of 1 s yielded a 25% and 42% larger bias compared to the other schemes, for 3DRP and OSEM respectively, and a parameter uncertainty that was 10-70% higher. The schemes from 4 to 15 s were generally not significantly different in regards to bias and SD. Typically, the reconstruction method 3DRP yielded less frame sampling dependence and less uncertain results compared to OSEM, but was on average more biased.

Conclusion: Of the six sampling schemes investigated in this study, an early frame duration of 6-15 s generally kept both bias and uncertainty to a minimum, for both 3DRP and OSEM reconstructions. Very short frames of 1 s should be avoided since they typically resulted in the largest parameter bias and uncertainty. Furthermore, 3DRP may be preferred over OSEM for short frames with poor statistics.

Key words: Dynamic PET, Monte Carlo, GATE, compartment modeling, frame sampling

INTRODUCTION

Positron emission tomography (PET) is a widely used and powerful tool for the quantitative *in vivo* study of radiolabeled molecules (tracers). In quantitative PET imaging, it is important to understand and quantify random (uncertainty) and systematic (bias) errors that will affect the quantitative information within an image set. Although there have been many studies focused on the bias and uncertainty of model parameter estimates (1,2), the effect of the early frame duration on these quantities is less understood.

Many early studies regarding optimal frame sampling schedules are mainly focused on the blood assay sampling for input function determination or reducing the computational time and storage space of dynamic image sets (3–6). Raylman et al. (7) studied protocols for dynamic cardiac imaging with different early frame samplings from 60 down to 5 s, and concluded that the first 100 s of the acquisition have to be sampled at 5 or 10 s for an acceptable bias in K_1 and k_2 for the 1-tissue compartment model. Jovkar et al. (8) investigated schemes with the first three minutes sampled at combinations of 10, 30 and 60 s, and found that parameter standard deviation (SD) decreased with decreased frame sampling (down to 10 s).

These studies only included frame sampling intervals down to 10 s, or occasionally 5 s, however. Moreover, the studies employed calculated time-activity curves (TACs) and used either the theoretical TACs directly or, to resemble real clinical data, added noise according to a Poisson or Gaussian distribution. Although the noise in projection data (sinograms) is Poisson distributed, the distribution is usually much more complex after the reconstruction process, especially for nonlinear iterative reconstruction algorithms (9,10). In order to avoid making assumptions and simplifications regarding the camera system blurring effect and noise distribution on the PET image level, a more sophisticated simulation method is needed. By using Monte Carlo (MC) techniques one can obtain images with realistic noise distributions and proper camera system effects.

The ^{18}F -labeled molecule 2-deoxy-2- (^{18}F) fluoro-D-glucose (^{18}F -FDG) is the most commonly used PET tracer in general and for tumor imaging in particular (11). Other tracers however, such as 3'-deoxy-3'- (^{18}F) fluorothymidine (^{18}F -FLT), have proven successful alternatives to ^{18}F -FDG for brain tumor studies

(11–14). This work focused on the tracer ^{18}F -FLT, which can be used to image tumor proliferation (11–14).

In dynamic PET, the tracer distribution over time is observed. The collected projection data are sorted into frames from which the kinetics of the tracer in a tissue or organ of interest can be quantified. Commonly, the dynamic data are analyzed using a tracer-specific compartment model, yielding a set of model-determined parameters representing the tracer kinetics. For dynamic PET imaging, list-mode data can be collected and binned to arbitrary frame durations. When reconstructing the data into a dynamic image set, the user is faced with the choice of using longer frames with better counting statistics but poor temporal resolution, or shorter frames with poor counting statistics but better temporal resolution.

Short frames may be of interest during the first minutes of the dynamic PET study to better capture the fast variations in the tracer uptake and clearance, which are usually largest for early frames, and for a better definition of the early blood peak (6). This is especially true for image-derived time-activity curves (TACs) of the blood, since they are sharper than the TACs of the tissue, and thus require higher sampling rates (7). Clinical PET frames are often sampled at intervals ranging from 10 s to 300 s, although frames shorter than 5 s exist but are rare. Although short frames are often desired in dynamic PET imaging, they are seldom used due to the poor statistics associated with short frames and poor quality and bias of image reconstructions of such frames (6).

The aim of this study was to investigate the effects different sampling schemes (frame durations) for early frames have on pharmacokinetic parameter estimates in regards to bias and SD for typical dynamic ^{18}F -FLT brain studies with typical dose administrations (noise level). The aim was also to investigate the effect of the reconstruction method used for the dynamic PET data by comparing the results for analytical three-dimensional (3D) filtered back-projection with reprojection (3DRP) and 3D ordered-subset expectation maximization (OSEM). To obtain data, the MC software GATE was used to simulate 2×15 separate dynamic PET studies with a digital head phantom with added tumors, representing ^{18}F -FLT with realistic kinetic parameter values.

MATERIALS AND METHODS

Compartment model

The 2-tissue compartment model seen in Fig.1 is commonly used to describe ^{18}F -FLT (15). The TAC describing the activity concentration in arterial blood is known as the input function C_p , and the two TACs describing the tissue concentrations C_{F+NS} and C_S represent free plus nonspecific (nondisplaceable) and specifically bound tracer in tissue, respectively. The model parameters that govern the tracer exchange are: the uptake rate from blood to nondisplaceable tracer in tissue K_1 ($\text{ml cm}^{-3} \text{ min}^{-1}$), the clearance rate from nondisplaceable tracer in tissue k_2 (min^{-1}) and the rates between the nondisplaceable and specifically bound tracer tissue compartments k_3 (min^{-1}) and k_4 (min^{-1}), respectively. V_a (ml cm^{-3}) is the fraction of arterial blood in tissue. The influx rate constant K_i ($\text{ml cm}^{-3} \text{ min}^{-1}$) is commonly used when evaluating dynamic data, and is defined as (8,12,15):

$$K_i = \frac{K_1 k_3}{k_2 + k_3}. \quad (1)$$

The activity measured by the PET camera is the sum of C_{F+NS} and C_S , plus an added blood component to account for signal contamination from blood vessels within the voxel or a volume-of-interest (VOI) (8,16,17).

Monte Carlo simulation

GATE (18) was used to perform MC simulations of 3D dynamic PET ^{18}F -FLT brain scans. The camera simulated was a previously validated GE Discovery LS PET scanner (19), consisting of 18 detection rings with 672 bismuth germanate (BGO) crystals of approximate size $4 \times 8 \times 30$ mm each. The transaxial field-of-view was 550 mm and the axial field-of-view 152 mm.

The phantom used in the simulations was the voxelized digital BrainWeb head phantom (20). The phantom was simulated and described in a previous study (21), and is briefly described here. The phantom consisted of seven main materials, with seven uniform spherical tumors (diameters 3, 6, 9, 12, 18, 24, and 30 mm) distributed in each hemisphere (14 inserted tumors). Finally, a 25 mm spherical blood region was

placed centrally in the brain. The constructed phantom had an isotropic voxel size of $1 \times 1 \times 1$ mm, and is depicted in Fig. 2. The size, shape, and location of the blood region was designed to be practical for extraction of an image-derived input function of small variance and little influence of partial volume effects, rather than to be realistic. Furthermore, inclusion of a blood region within the phantom eliminated the need for additional simulations (of e.g. the heart) for input-function derivation.

Realistic pharmacokinetics was assigned to all normal phantom tissues, and fitted TACs from two clinical dynamic brain FLT scans performed at Umeå University Hospital were used for those regions. The same input function C_p was assigned to the blood region in both setups, denoted FLT_1 and FLT_2 . C_p was generated using Matlab (v. 8.1.0, The MathWorks Inc., MA, USA), and had a typical input function appearance (22) with a realistic peak amplitude of around 50 kBq/cc (measured at Umeå University Hospital). For each of the two setups, Matlab was used to generate the corresponding TTAC C_{PET} , according to the 2-tissue model with the realistic ^{18}F -FLT parameter values for gliomas, seen in Table 1 (12,13). For both FLT_1 and FLT_2 , all 14 tumor regions were assigned the same TTAC C_{PET} . The simulated blood and tumor TACs are seen in Fig. 3. The source particles simulated were ^{18}F positrons with an electron range production cut of 2 mm, a δ -ray production cut of 10 keV, and an x-ray production cut of 10 keV (19,23). Physical decay of the sources was applied with a half-life of 6586.2 s. The activities in the tissue- and blood regions of the phantom were read from the generated TACs and updated every second of the simulation. For practical reasons the detector dead time was not included in the simulation. The total GATE acquisition time was set to 60 min and simulated data were stored in list-mode. A total of 30 MC simulations were performed; 15 of the setup with FLT_1 and 15 with FLT_2 , in order to improve the statistics for the kinetic parameter analyses. Although simulated, the random coincidences were not included in the study. The effect of random coincidences was considered small as the random fraction for the two setups was merely 2%.

As previously described in (21), data from one normalization and one calibration simulation were also used for the image reconstruction normalization and quantitative calibration.

All simulations were performed using the computer cluster Akka (Intel Xeon quad-core L5420 central processing units) at the HPC2N collaboration, Umeå University. Each of the 30 dynamic simulations required a total of about 3300 central processing unit hours.

Image reconstruction

The list-mode true+scattered coincidences were binned into 3D sinograms (19) and reconstructed using two methods: Analytical 3DRP (24) and OSEM (25) iterative reconstruction. The reconstructions were performed using the software STIR (26). A Colsher filter (cut-off frequency 0.5 pixel^{-1}) was applied for 3DRP and the OSEM settings were chosen so that the tumor VOI values had reached convergence at 60 subiterations and 12 subsets (5 iterations). Both methods had normalization, decay, attenuation, and scatter corrections applied.

For the attenuation correction, a linear attenuation coefficient data map (μ -map) relevant for 511 keV photons for the respective phantom materials was generated from the BrainWeb phantom. The normalization simulation data were binned into a sinogram to create the normalization sinogram (27). A scatter sinogram estimate was created from the single scatter simulation (SSS) algorithm implemented in STIR (28,29), and used as additive sinograms in the OSEM loop. Attenuation and normalization data were also included in the loop, whereas all three corrections were used as pre-corrections for 3DRP.

In accordance with clinical settings of the GE Discovery LS, all reconstructed images were post-filtered with a 6.0 mm FWHM Gaussian transverse filter and a 3-point smoothing filter $[1 \ 2 \ 1] / 4$ in the axial direction. Reconstructed image sizes were $165 \times 165 \times 35$ voxels with a voxel size of $2 \times 2 \times 4.25$ mm.

Finally, a scale factor to calibrate all images from counts to Bq/ml was created from a 3DRP reconstruction of the true coincidences from the calibration simulation.

The dynamic PET data were reconstructed into six dynamic image sets, with the first two minutes (covering the early blood peak) sampled at 120×1 s, 60×2 s, 30×4 s, 20×6 s, 12×10 s, or 8×15 s. The PET data between 2 and 60 min were all sampled at 2×30 s, 2×60 s, 2×150 s, and 10×300 s.

Model fitting and parameter analysis

The input function was image-derived from a spherical VOI covering the complete blood region (25 mm diameter, 488 voxels, 8.3 ml), and two tumor TTACs from each simulation were derived from complete VOIs of the largest left and right tumors, respectively (30 mm diameter, 843 voxels, 14.3 ml). In this study, only the two largest 30 mm tumors were used in order to minimize partial volume effects (the additional 12 tumor spheres are intended for another study). The data used for analysis thus comprised 15 input functions and two TTACs per input function, making a total of 30 tumor TTACs for each of FLT₁ and FLT₂, where the TAC values were calculated as the mean value of the VOI at each frame.

Kinetic parameter estimates were obtained by nonlinear-least-squares (NLS) fitting of each of the TTACs with the input function considered a noiseless model input. The NLS fitting is commonly weighted, and each TTAC value should be weighted according to its inverse variance. Since the true variance is typically unknown, it is usually approximated by considering radioactive decay, frame duration and often also frame count. However, weighting according to noisy counts can degrade the parameter estimation severely (30,31). Furthermore, in order not to force a fit only to the last few TTAC values with long frame durations and in essence ignore the short early frames, a uniform weight was used for all frames in this study. The Matlab function `lsqnonlin` was used for the fitting, and the true values were used as start values to avoid any effects from the choice of initial parameter guesses. The midtime of each frame was used as the time point and the influx rate parameter K_i was calculated according to Eq. 1 for each VOI.

The 30 sets of kinetic parameters were finally averaged into one single set of estimated [$K_1, k_2, k_3, k_4, V_a, K_i$] for each of the six sampling schemes, for both FLT₁ and FLT₂. The relative bias of all six pharmacokinetic parameter estimates P was calculated as

$$(P - P_{true}) \times \frac{1}{P_{true}} \times 100(\%), \quad (2)$$

where P_{true} is the true parameter value. The accompanying relative standard error in the bias was

$$\frac{SP}{\sqrt{30}} \times \frac{1}{P_{true}} \times 100(\%), \quad (3)$$

where s_p is the SD of parameter estimate P. The relative SD in the parameter estimates was calculated according to

$$s_p \times \frac{1}{P_{true}} \times 100(\%). \quad (4)$$

The theoretical, noiseless input functions and TTACs, resampled to match the six different frame sampling schemes, were also NLS fitted and compared to the results from the image-derived TACs.

The obtained biases were analyzed with 1- and 2-way ANOVA tests, followed by post-hoc Bonferroni pairwise tests to make out individual differences between reconstruction methods and sampling schemes. Results with $p < 0.05$ were considered significant.

All data fitting and analyses were performed in Matlab.

RESULTS

On average, the total registered and kept coincidences from the 15 simulations was 119×10^6 and 137×10^6 , for FLT₁ and FLT₂, respectively. The total kcounts per frame for the early frames (first 120 s) of the different sampling schemes are seen in Table 2.

Examples of the reconstructed images are seen in Fig. 4, and representative TTACs from one of the 30 FLT₁ tumor VOIs, with corresponding NLS fit are seen in Fig. 5. As can be seen in both figures, the noise level of the images and subsequent TACs decreases as the frame duration increases. The calculated bias and SD of the parameter estimates from the NLS fits of the image-derived input function and TTAC are seen in Fig. 6, and the results for the resampled theoretical (noiseless) TACs (nonclinical case used merely for comparison) are seen in Fig. 7.

The shortest early sampling of 1 s generally produced the most biased parameter estimates, and more so for OSEM compared to 3DRP reconstructions. On average, the 1 s parameter bias magnitudes were 25% and 43% larger than the other sampling schemes, for 3DRP and OSEM respectively. Due to parameter uncertainties however, the results were only significant for parameters K_1 , k_2 , and V_a with OSEM (both FLT setups), K_1 and k_2 for FLT₂ with 3DRP, and V_a for both FLT setups with 3DRP. The 2 s scheme also

yielded significantly larger biases compared to the longer schemes for parameters K_1 and k_2 with OSEM. In general, the sampling schemes of 4, 6, 10 and 15 s did not differ significantly, with the exception of V_a with 3DRP where most schemes differed from one another. From Fig. 7 (theoretical, noiseless TACs) it is apparent that V_a is the parameter most dependent on frame sampling.

On average, parameter k_3 was the least biased estimate at 4% on average for all schemes, and 3% when excluding the 1 s scheme. Its bias from 2 to 15 s sampling was in fact not significantly different from the theoretical case at around 2%.

The minimum bias magnitude was found between 6 and 15 s early frame sampling for both FLT setups for all six parameters, and both reconstruction methods. The minimum typically occurred at a shorter sampling of 6 s for 3DRP and about 15 s for OSEM. Note however that the schemes of 4, 6, 10 and 15 s were generally not significantly different.

Parameter estimate uncertainties (SDs) were generally stable for an early frame sampling of 2 to 15 s, but increased by 10-70% when shortening it to 1 s. The uncertainty was smallest for parameter K_1 with an average of 4%, and largest for k_4 at 25%.

Comparing the significant results of the two reconstruction methods, 3DRP produced more biased estimates of K_1 , k_2 , and V_a compared to OSEM, by 44%, 92% and 314%, and a less biased k_4 by 8%. Uncertainties however were larger for OSEM reconstructions by on average 15%.

DISCUSSION

In this study, we investigated the effect of early frame duration on bias and SD in pharmacokinetic parameter estimates obtained from the 2-tissue compartment model for typical ^{18}F -FLT brain studies.

Two sets of kinetic parameter value sets were chosen, representing the tracer ^{18}F -FLT, but since the simulations themselves were parameter specific, not tracer specific, the results are likely valid for any tracer suited for the 2-tissue compartment model with similar pharmacokinetic parameter values and noise level (dose administration). Two image reconstructions methods were also studied, 3DRP and OSEM.

Of the statistically significant results, the bias was generally smallest for early frame durations of 6-15 s. A frame sampling dependence was generally found for K_1 , k_2 , V_a , and more so for OSEM than 3DRP. The closer statistical analysis revealed that it was the 1 s, and occasionally also the 2 s scheme that stood out from the rest. With 3DRP, it was only for the faster kinetics described by FLT_2 that a frame sampling dependence was found for K_1 and k_2 . The slower kinetics in FLT_1 did not show a significant sampling dependence. These results are not surprising as faster kinetics should intuitively be more prone to undersampling than slower kinetics where the TACs do not vary as quickly from frame to frame. Parameter K_1 mainly governs the amplitude of the TTAC, whereas k_2 , k_3 and k_4 together contribute to the shape of the TTAC. This makes predictions regarding individual parameter responses to changes in the TTAC shape difficult. Apart from the highest bias, the SDs were also highest for the shortest frames of 1 s. This is expected since the signal-to-noise ratio of the frames is roughly proportional to the square root of the number of counts.

The bias for OSEM appeared to have a frame duration dependence which was more pronounced than for 3DRP, for parameters K_1 and k_2 . It is known that iterative reconstruction (OSEM) of low-count images may result in (positively) biased images whilst analytical reconstruction methods (3DRP) do not (32,33). The bias introduced due to low count reconstruction may explain the larger bias for short frames, and hence more prominent frame duration dependence for OSEM compared to 3DRP. The parameter K_1 which mainly controls the peak amplitude of the TTAC would thus be most affected by a biased ROI value. Compared to OSEM, 3DRP images have a high background noise and streak artifacts (Fig. 4). It should be noted however that the lowest count OSEM images (1 s and 2 s frames) appear to have artifacts in the form of high uptake spots. The effect of the low count bias for short framed OSEM images and how it transfers to the parameter biases and SDs is very hard to include properly in studies where the TACs are simulated directly with added noise profiles. This effect is a lot more realistically depicted using full MC simulations with complete image reconstructions.

Furthermore, according to typical practice, the same setting (here 60 subiterations, 12 subsets) was used for all frame sampling schemes and for all frames of each scheme. However, because of the difference in

statistics between the different frames, they should ideally (despite practicality issues), have the OSEM reconstruction settings optimized individually. Furthermore, OSEM images have noisier hot regions than 3DRP, and vice versa for cold regions, as known from literature (9,34). Cerebellum VOI (cold) SDs and tumor VOI (hot) SDs were on average 71% higher and 28% lower, respectively, when comparing 3DRP to OSEM. This fact, together with the low count bias may explain the 15% larger parameter uncertainties obtained for OSEM compared to 3DRP images. However, the noise level in OSEM images is heavily dependent on the number of iterations, and other reconstruction settings could yield slightly different results.

It is apparent that V_a is dependent on the frame duration. Even the theoretical TACs (Fig. 7) resulted in large biases for the longer sampling intervals. Since V_a is determined by the early blood peak seen in the TTAC, a long frame duration will effectively lower the peak due to smearing and cause an underestimated V_a . An input function with a wider peak would most likely decrease the frame sampling dependence and yield less bias in V_a . On the other hand, a more narrow blood peak would likely cause V_a to be more underestimated.

Both k_3 and K_i was found independent of early frame sampling. Even though Fig. 6 shows a larger bias for the shortest 1 s frame sampling, the results were not significant. These two parameters have been shown to be of potentially larger clinical value (13,14), so a small dependence on frame sampling scheme is desired. As K_i is a macro parameter calculated from three other parameters, it is likely to be more stable than single parameters (6). The image-derived k_3 was not different from the theoretical noiseless case. Thus, the effects of the camera system blurring, reconstruction process etc. did not add additional bias to the estimate. This makes it reliable and strengthens its role as a clinically relevant parameter.

The bias and SD of parameter k_4 was large. A longer scan time (>60 min) would likely improve the k_4 estimation (15), but as this parameter is rarely considered clinically important due to large uncertainties, we chose not to take this into further consideration. Jovkar et al. (8) found that keeping k_4 fixed in the fitting procedure resulted in more stable estimates of all other parameters.

According to our findings, noise and bias in the image-derived TACs can affect the parameter uncertainty and bias to a large extent. Since the input function is derived from only one ROI and assumed true for the fitting procedure, any bias in it will affect all parameter estimates. If the chosen blood ROI is not representative, the calculated bias and SD in the parameter estimates may be largely affected. To minimize uncertainty and bias the use of a population based input function might be helpful (22,35). It should be noted however that the population based input function is subject to interpatient variability and may be biased in itself.

The parameter bias was found larger for 3DRP than OSEM, and the uncertainty smaller on average. As shown by Thiele et al. (31) and Yaqub et al. (30), the choice of weight factors for weighted NLS can affect the results to a relatively large extent. In addition to uniform weighting, the fitting and subsequent parameter analyses were also done with two standard weight estimations (31) (data not shown). For the i^{th} frame in each set, the two weights w_i were calculated as:

$$w1_i = F_i \times \frac{e^{-\lambda t_i}}{TAC_i}, \quad (5)$$

and

$$w2_i = F_i \times e^{-\lambda t_i}, \quad (6)$$

where F_i is the frame duration, t_i the frame midtime, λ the decay constant and TAC_i the TAC value of the i^{th} frame. The results when including either of the weights were on average worse than with uniform weighting. We therefore chose not to present these results. Worth mentioning however is that although we found OSEM to produce less biased parameter estimates when using uniform weighting, when using either $w1$ or $w2$, 3DRP yielded considerably better estimates than OSEM. The bias for OSEM reconstructions benefited from uniform weighting, whereas 3DRP showed minimum bias for $w1$.

The size of the tumor ROIs were set to 14.3 ml in this study, which is a realistic volume for a brain tumor ROI. The ROI size and the image noise level (activity) will affect the results since a larger ROI or higher activity yields better statistics. In this study the focus was to evaluate a typical ^{18}F -FLT study and administered dose (noise level) and kinetic parameter values were chosen accordingly. For a more general

understanding of the parameter biases and uncertainties in relation to noise level and pharmacokinetics, a full range of different dose administrations and parameter value sets could be simulated and analyzed.

Finally, when comparing FLT_1 and FLT_2 , it is clear that the magnitudes of both bias and SD are often different, reflecting the difference in parameter reliability on the individual patient level as there is a wide range of clinically possible kinetic parameter values.

CONCLUSION

In general for this study, an early frame sampling of 6-15 s was found to minimize the overall bias in pharmacokinetic parameters for both 3DRP and OSEM reconstructions. Parameters K_1 , k_2 and V_a showed a statistically significant frame sampling dependence with the largest bias for the shortest frames of 1 s, and more so for OSEM compared to 3DRP. The parameter uncertainties were generally stable for frames of 2-15 s, but higher for the short 1 s sampling.

The estimation of k_3 was most reliable (bias <5% in general), and the parameter V_a was overall most dependent on frame duration.

Despite the visually more appealing OSEM images, the analytic image reconstruction method 3DRP showed less dependence on early frame sampling, compared to the iterative technique OSEM. Moreover, OSEM reconstructions of the shortest early frames (1 and 2 s) had artefacts in the form of high uptake spots, not seen in the 3DRP images.

ACKNOWLEDGMENTS

The authors would like to thank Prof. Jun Yu from the Department of Mathematics and Mathematical Statistics at Umeå University for his support on statistical calculations. This work was supported in part by the Swedish Cancer Society and the Cancer Research Foundation at Umeå University.

REFERENCES

1. Doot RK, Scheuermann JS, Christian PE, Karp JS, Kinahan PE. Instrumentation factors affecting variance and bias of quantifying tracer uptake with PET/CT. *Med Phys*. 2010;37:6035–46.
2. Kamasak ME. Computation of variance in compartment model parameter estimates from dynamic PET data. *Med Phys*. 2012;39:2638–48.
3. Li X, Feng D. Optimal design of scan intervals for glucose kinetic modeling using dynamic imaging data from PET. IEEE Conference Record of IEEE Engineering in medicine and biology (Baltimore), 1994;634–5.
4. Cai W, Feng D, Fulton R. A fast algorithm for estimating FDG model parameters in dynamic PET with an optimised image sampling schedule and corrections for cerebral blood volume and partial volume. *IEEE Eng Med Biol Soc*. 1998;20:767–70.
5. D'Argenio DZ. Optimal sampling times for pharmacokinetic experiments. *J Pharmacokinet Biopharm*. 1981;9:739–56.
6. Li X, Feng D, Chen K. Optimal image sampling schedule for both image-derived input and output functions in PET cardiac studies. *IEEE Trans Med Imaging*. 2000;19:233–42.
7. Raylman RR, Caraher JM, Hutchins GD. Sampling requirements for dynamic cardiac PET studies using image-derived input functions. *J Nucl Med*. 1993;34:440–7.
8. Jovkar S, Evans AC, Diksic M, Nakai H, Yamamoto YL. Minimisation of parameter estimation errors in dynamic PET : choice of scanning schedules. *Phys Med Biol*. 1989;34:895–908.
9. Barrett HH, Wilson DW, Tsui BMW. Noise properties of the EM algorithm: I. Theory. *Phys Med Biol*. 1994;39:833–46.
10. Razifar P, Sandström M, Schneider H, et al. Noise correlation in PET, CT, SPECT and PET/CT data evaluated using autocorrelation function: a phantom study on data, reconstructed using FBP and OSEM. *BMC Med Imaging*. 2005;5:1–23.
11. Gulyás B, Halldin C. New PET radiopharmaceuticals beyond FDG for brain tumor imaging. *Q J Nucl Med Mol Imaging*. 2012;56:173–90.
12. Schiepers C, Dahlbom M, Chen W, et al. Kinetics of 3'-deoxy-3'-18F-fluorothymidine during treatment monitoring of recurrent high-grade glioma. *J Nucl Med*. 2010;51:720–7.
13. Schiepers C, Chen W, Dahlbom M, et al. 18F-fluorothymidine kinetics of malignant brain tumors. *Eur J Nucl Med Mol Imaging*. 2007;34:1003–11.
14. Spence AM, Muzi M, Link JM, et al. NCI-sponsored trial for the evaluation of safety and preliminary efficacy of 3'-deoxy-3'-[18F]fluorothymidine (FLT) as a marker of proliferation in patients with recurrent gliomas: preliminary efficacy studies. *Mol imaging Biol*. 2009;11:343–55.

15. Muzi M, Mankoff DA, Grierson JR, et al. Kinetic modeling of 3'-deoxy-3'-fluorothymidine in somatic tumors: mathematical studies. *J Nucl Med.* 2005;46:371–80.
16. Ikoma Y, Watabe H, Shidahara M, Naganawa M, Kimura Y. PET kinetic analysis: error consideration of quantitative analysis in dynamic studies. *Ann Nucl Med.* 2008;22:1–11.
17. Lodge MA, Carson RE, Carrasquillo JA, et al. Parametric images of blood flow in oncology PET studies using [¹⁵O]water. *J Nucl Med.* 2000;41:1784–92.
18. Jan S, Santin G, Strul D, et al. GATE: a simulation toolkit for PET and SPECT. *Phys Med Biol.* 2004;49:4543–61.
19. Schmidtlein CR, Kirov AS, Nehmeh SA, et al. Validation of GATE Monte Carlo simulations of the GE Advance/Discovery LS PET scanners. *Med Phys.* 2006;33:198–208.
20. Collins DL, Zijdenbos AP, Kollokian V, et al. Design and construction of a realistic digital brain phantom. *IEEE Trans Med Imaging.* 1998;17:463–8.
21. Häggström I, Schmidtlein CR, Karlsson M, Larsson A. Compartment modeling of dynamic brain PET - The impact of scatter corrections on parameter errors. *Med Phys.* 2014;41:111907–1–9.
22. Contractor KB, Kenny LM, Coombes CR, et al. Evaluation of limited blood sampling population input approaches for kinetic quantification of [¹⁸F]fluorothymidine PET data. *Eur J Nucl Med Mol Imaging.* Springer Open Ltd; 2012;2:1–11.
23. Mitev K, Gerganov G, Kirov AS, et al. Influence of photon energy cuts on PET Monte Carlo simulation results. *Med Phys.* 2012;39:4175–86.
24. Kinahan PE, Rogers JG. Analytic 3D image reconstruction using all detected events. *IEEE Trans Nucl Sci.* 1989;36:964–8.
25. Hudson HM, Larkin RS. Accelerated image reconstruction using ordered subsets of projection data. *IEEE Trans Med Imaging.* 1994;13:601–9.
26. Thielemans K, Tsoumpas C, Mustafovic S, et al. STIR: software for tomographic image reconstruction release 2. *Phys Med Biol.* 2012;57:867–83.
27. Schmidtlein CR, Turner A, Nehmeh SA, et al. SU-FF-I-54: A Monte Carlo Model of the Discovery ST PET Scanner. *Med Phys.* 2006;33:2009.
28. Thielemans K, Sauge D, Labbé C, et al. Software for tomographic image reconstruction user's guide v2.1. 2011. p. 1–67.
29. Tsoumpas C, Aguiar P, Nikita KS, Ros D, Thielemans K. Evaluation of the single scatter simulation algorithm implemented in the STIR library. *IEEE Conference Record of IEEE Nuclear Science Symposium Conference (Rome),* 2004;3361–5.
30. Yaqub M, Boellaard R, Kropholler MA, Lammertsma AA. Optimization algorithms and weighting factors for analysis of dynamic PET studies. *Phys Med Biol.* 2006;51:4217–32.

31. Thiele F, Buchert R. Evaluation of non-uniform weighting in non-linear regression for pharmacokinetic neuroreceptor modelling. *Nucl Med Commun*. 2008;29:179–88.
32. Reilhac A, Tomei S, Buvat I, et al. Simulation-based evaluation of OSEM iterative reconstruction methods in dynamic brain PET studies. *Neuroimage*. 2008;39:359–68.
33. Walker MD, Julyan PJ, Talbot PS, Jones T, Matthews JC. Bias in iterative reconstruction of low-statistics PET data: benefits of a resolution model. IEEE Conference Record of IEEE Nuclear Science Symposium Conference (Orlando), 2009;2857–63.
34. Boellaard R, van Lingen A, Lammertsma AA. Experimental and clinical evaluation of iterative reconstruction (OSEM) in dynamic PET: quantitative characteristics and effects on kinetic modeling. *J Nucl Med*. 2001;42:808–17.
35. De Geus-Oei L-F, Visser EP, Krabbe PFM, et al. Comparison of image-derived and arterial input functions for estimating the rate of glucose metabolism in therapy-monitoring 18F-FDG PET studies. *J Nucl Med*. 2006;47:945–9.

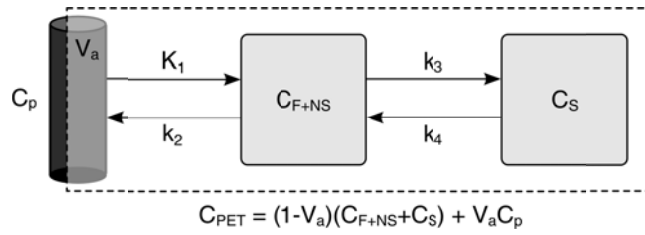


FIGURE 1. The 2-tissue compartment model consisting of compartments of arterial blood plasma (C_p), free plus nonspecific (nondisplaceable) and specifically bound tracer in tissue (C_{F+NS} and C_S) as well as four rate constants (K_1, k_2, k_3, k_4) and the tissue blood fraction (V_a). C_{PET} is the apparent concentration in a PET image VOI or voxel.

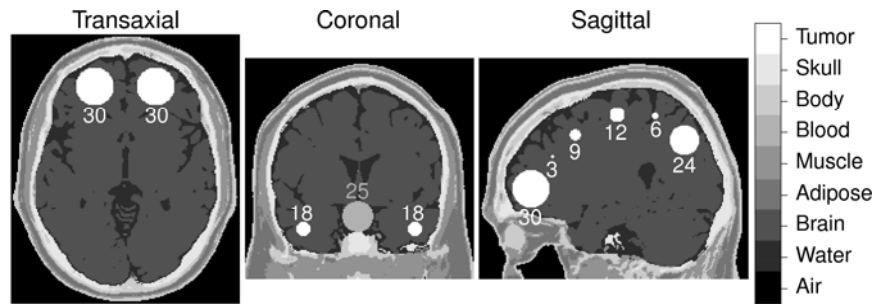


FIGURE 2. The voxelized BrainWeb head phantom, with inserted spherical blood and tumor regions, labeled with their diameter in mm. All tissues were attributed realistic TACs, and the blood region was assigned the input function (C_p) and all 14 tumor regions the same TTAC (C_{PET}).

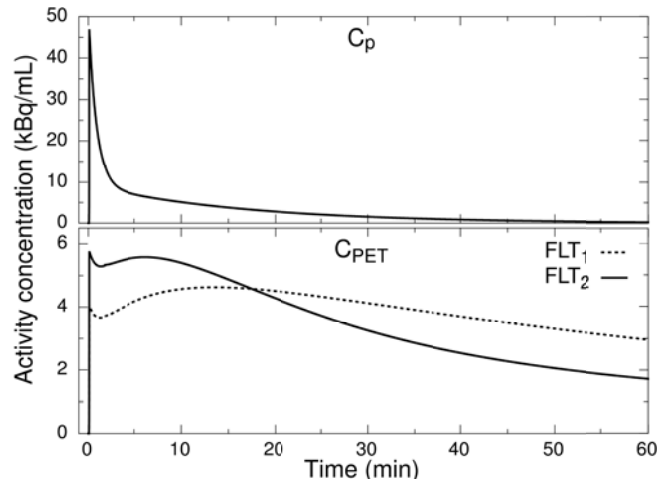


FIGURE 3. The common input function C_p (top) and C_{PET} for the two ^{18}F -FLT parameter sets (bottom), showing the activity concentration for the blood and tumor regions, respectively.

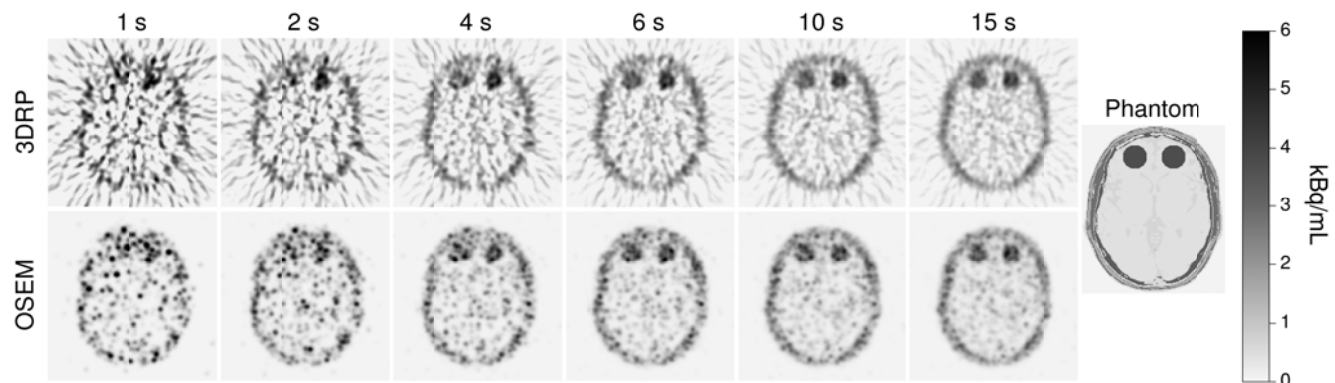


FIGURE 4. Example images from the FLT_1 study, for the different early frame sampling schemes plus the true phantom image. The frame around 120 s is presented and the early frame durations are indicated in the columns of the figure. Top row: 3DRP, bottom row: OSEM.

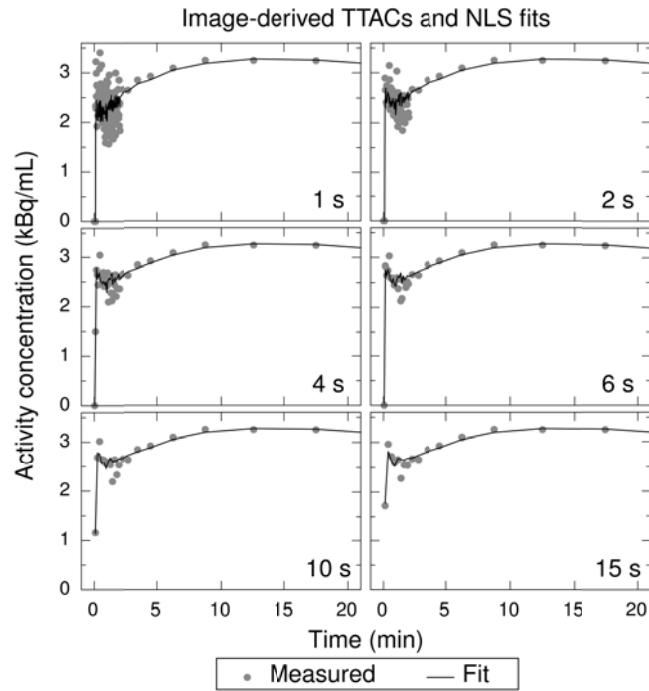


FIGURE 5. Representative example from the first 20 min of the FLT₁ study, showing OSEM TTACs and corresponding NLS fits for the six different early frame sampling schemes.

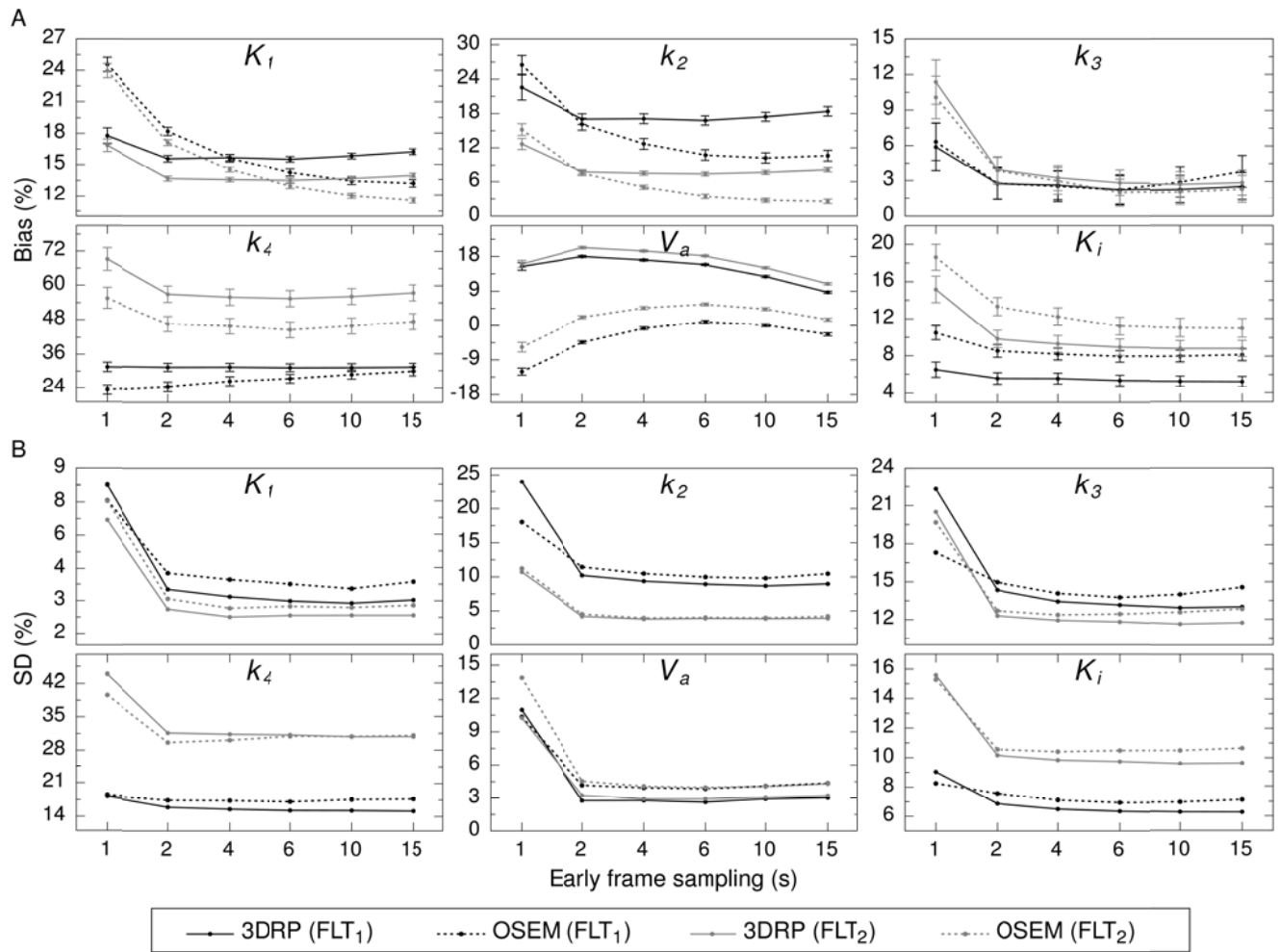


FIGURE 6. Relative A) error (bias) and B) uncertainty (standard deviation, SD) in all parameter estimates for the six different early frame sampling schemes. The error bars in the bias represent the standard error.

Note that the y-axes are scaled differently for better visibility.

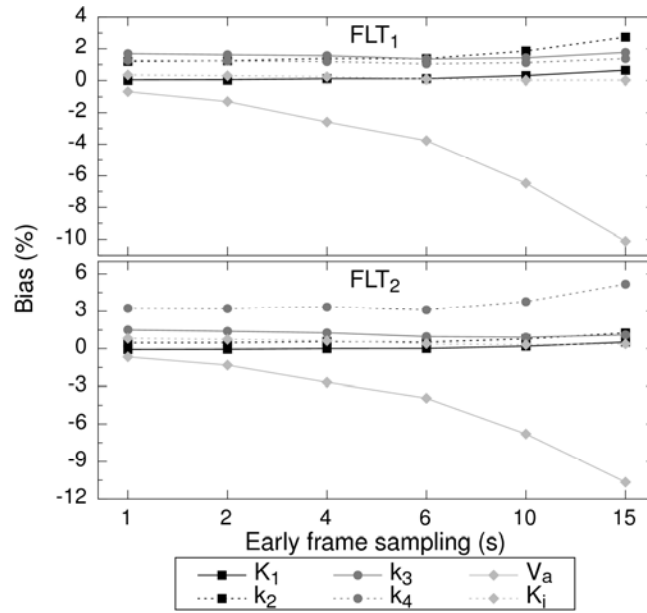


FIGURE 7. Relative bias for all model parameters for the six different early frame sampling schemes, using the resampled theoretical (noiseless) input function and TTAC for the NLS fit.

TABLE 1. The two sets of simulated ^{18}F -FLT parameter values; FLT₁ (12) and FLT₂ (13).

	K_1	k_2	k_3	k_4	V_a	K_i^*
FLT ₁	0.071	0.091	0.047	0.018	0.086	0.024
FLT ₂	0.111	0.131	0.017	0.012	0.122	0.013

* Values calculated by Eq. 1

TABLE 2. Total number of kcounts in the early frames (first 120 s of the acquisition) for the different sampling schemes.

	1 s	2 s	4 s	6 s	10 s	15 s
FLT ₁	0-44	0-87	0-173	3-258	125-429	282-642
FLT ₂	0-57	0-113	0-226	4-338	162-564	368-843